

## Flow Visualization of Internal Flow in the Human Lung Network

Brücker, Ch.\*<sup>1</sup> and Schröder, W.\*<sup>2</sup>

\*1 Chair of Fluid Mechanics and Fluid Machinery, TU Freiberg, 09599 Freiberg, Germany. E-mail: bruecker@imfd.tu-freiberg.de

\*2 Institute of Aerodynamics, RWTH Aachen, 52062 Aachen, Germany.

Received 24 November 2005

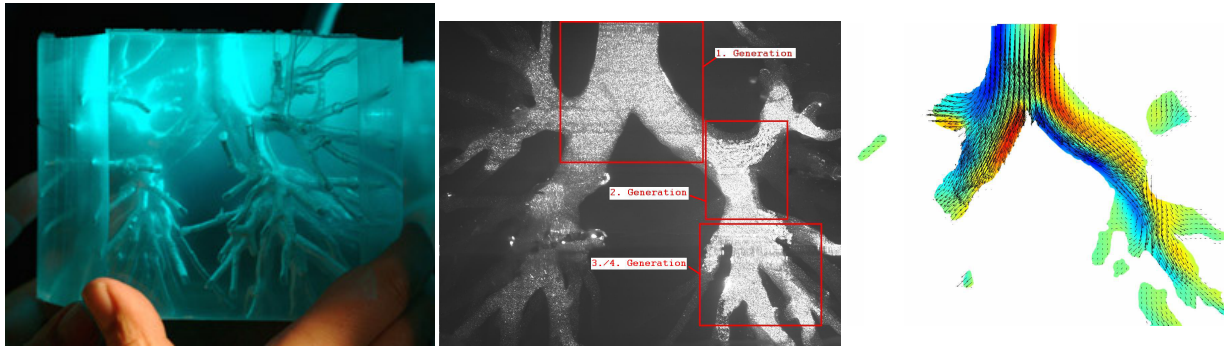


Fig. 1.

Figure 1 left shows a realistic transparent model of the human airways with the trachea at the top and 6 generations of branching representing the bronchial tube system of the lung. The model is a negative cast of a rapid prototyped kernel of the bronchial tree structure generated from a CT scan. After casting in transparent silicone, the kernel is dissolved and the bronchial tree is left as a hollow structure in the transparent silicone block. Flow studies are carried out in a pulsatile mock circuit with a mixture of water and glycerine as working fluid. The refractive index of the fluid is matched with the silicone model to visualize the internal flow structures by optical flow measurement techniques such as Particle-Image-Velocimetry (PIV).

The picture in Figure 1 at the center gives an impression of the tracer images in a light-sheet which crosses the vertical axis of the trachea. Hydrogen bubbles are used to visualize the flow. The light-sheet cuts a vertical plane across the major branch plane and extends down to branches in the 4<sup>th</sup> generation. An exemplary result of the PIV study is given in Figure 1 on the right hand side by means of the velocity field and vorticity distribution during inspiration. The results demonstrate the generation of separation regions and secondary vortex structures. As proven, the mean flow tends to follow the inner walls of the branching tubes.

## Shaping Converging Shock Waves by Means of Obstacles

Eliasson, V.\*, Apazidis, N\*. and Tillmark, N\*.

\* KTH Mechanics, SE-100 44 Stockholm, Sweden. E-mail: veronica@mech.kth.se

Received 9 January 2006

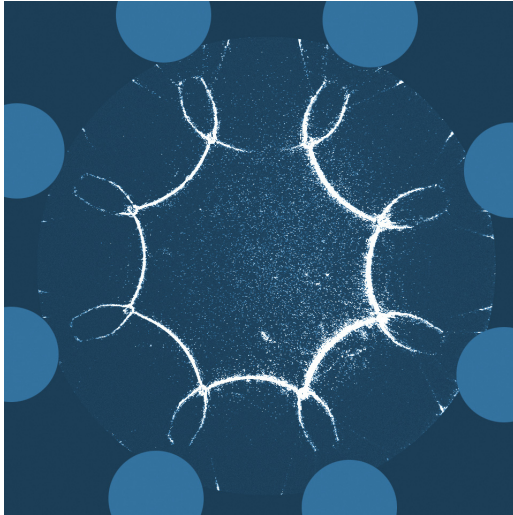


Fig. 1. A converging shock wave with concave sides in an octagonal pattern,  $t = t_0$ .

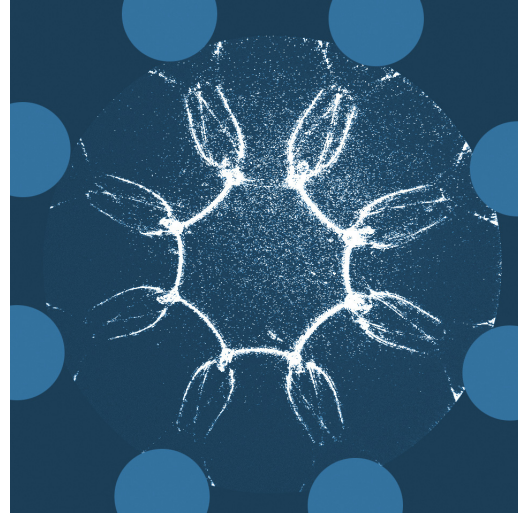


Fig. 2. Converging shock wave,  $t = t_0 + 5 \mu\text{s}$ .

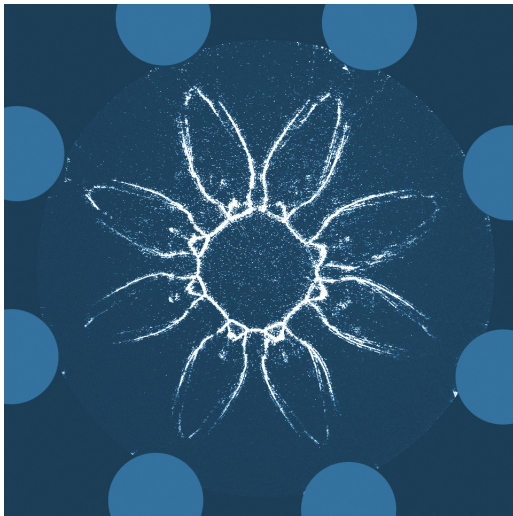


Fig. 3. Converging shock wave with 16 sides,  $t = t_0 + 10 \mu\text{s}$ .

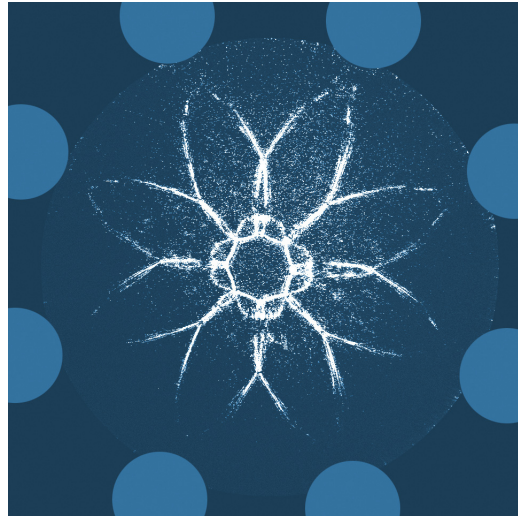


Fig. 4. Converging shock wave with 8 sides oriented opposite to Fig. 1,  $t = t_0 + 16.5 \mu\text{s}$ .

The schlieren photographs show a cylindrical converging shock wave at different time instants. Eight cylindrical obstacles, with diameters of 15 mm, are placed in an octagonal pattern to create octagonally shaped shock waves. At first, eight concave forward sides are created, Fig. 1 and 2. The concave sides will first get plane and then the shock wave will transform into a double octagon, Fig. 3. After some time it will transform back into an octagon again, with opposite orientation relative to the first one, Fig. 4. This behavior will repeat during the whole focusing process and depends on the nonlinear coupling between the local form of the shock front and the local propagation velocity.

## Visualization of Capillary Flow in Sessile Drops and Detecting Spreading Stability by Laser Refracted Shadowgraphy

Zhang, N.\*<sup>1</sup> and Chao, D. F.\*<sup>2</sup>

\*1 Ohio Aerospace Institute at NASA Glenn Research Center, Cleveland, OH 44135, USA.

E-mail: nzhang@grc.nasa.gov

\*2 Microgravity Division, NASA Glenn Research Center, Cleveland, OH 44135, USA.

Received 3 January 2006

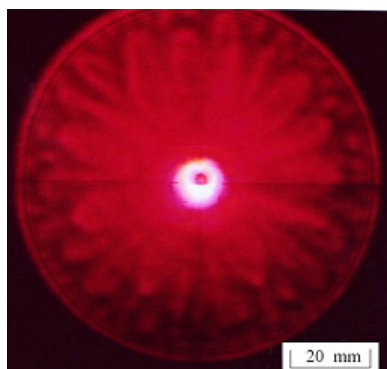


Fig. 1. The laser refracted shadowgraphic far-field image of an R-113 drop in the early stage of spreading shows multi-layer convection cells in the drop and a fold caustic with its caustic-diffraction fringes.

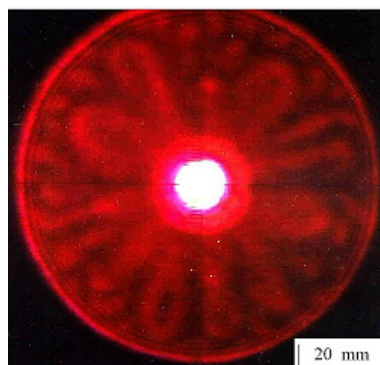


Fig. 2. In the last stage of the R-113 drop spreading, the shadowgraphic image shows single-layer convection cells in the drop and a fold caustic with its caustic-diffraction fringes.

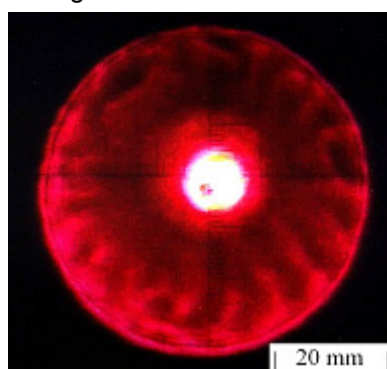


Fig. 3. Convection cells occur at the drop foot region in a spreading n-pentane drop while the fold caustic has a weak caustic diffraction.

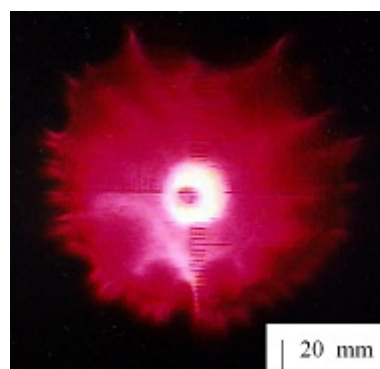


Fig. 4. No convection occurs in an ethanol drop but the drop surface creases to produce higher hierarchy of optical catastrophes.

When a parallel laser beam passes through a sessile liquid drop, the beam refracted by the drop and forms shadowgraphic image showing optical catastrophes in far field. This so-called laser refracted shadowgraphy can sensitively detect convective flow in a sessile drop, which is invisible to the naked eye, and spreading stability of the drop. These figures show the shadowgraphic images of a 5  $\mu\text{l}$  sessile drop of different liquids. A perfect circle image, as shown in Figs. 1-3, indicates that this kind of drops spreads stably and has a perfect circular three-phase-line and a perfect sphere-cap profile without wrinkle on the surface. Figures 1-3 show different flow patterns and indicate that the flows have no influence on the stability of spreading. The shadowgraphy is also very sensitive to the stability of spreading through the hierarchy of optical catastrophes. Figure 4 shows no flow in the drop but the spreading is unstable, manifested as an irregular circle image with saw-tooth-like ring consisting of cusps of caustic produced by a higher hierarchy of optical catastrophes. Much other important information, such as contact angle, drop profile, and height of the drop foot, can be obtained by optical calculations and catastrophic optics analysis.

## Flutter Modes of a Flexible Plate in an Air Flow

Souilliez, C.\*, Schouveiler, L\* and Eloy, L\*.

\* Institut de Recherche sur les Phénomènes Hors Equilibre, 49 rue Joliot-Curie, BP 146, F-13384 Marseille Cedex 13, France.

Received 9 February 2006

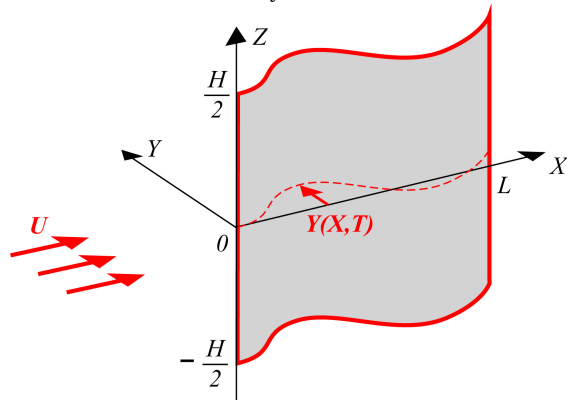


Fig. 1. Sketch of the experiment.

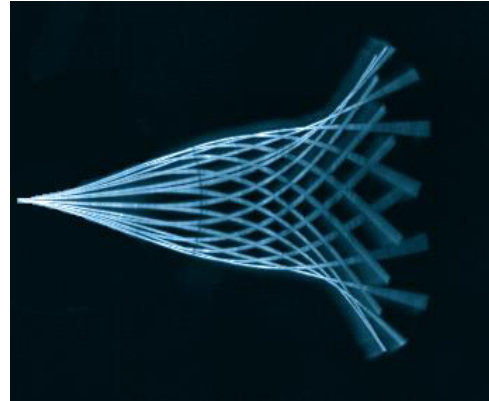


Fig. 2. Flutter for  $L = 8$  cm,  $U = 8$  m/s.

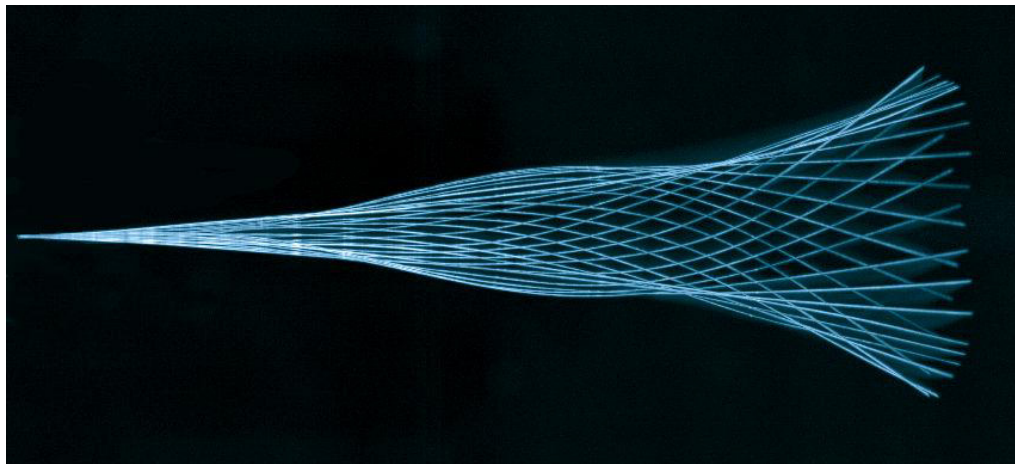


Fig. 3. Flutter for  $L = 21$  cm,  $U = 2.9$  m/s.

The flutter instability resulting from the interaction of a flexible plate with a fluid flow is experimentally investigated. The present visualizations are obtained with two square plates (i.e., of aspect ratio  $H/L = 1$ , see the sketch of the experiment in Fig. 1) made in a plastic sheet (of flexural rigidity  $4.8 \cdot 10^{-4} \text{ kg m}^2 \text{ s}^{-2}$ ) and of length  $L = 8$  and 21 cm. Experiments are performed in the horizontal test section of a low-turbulence wind tunnel. The upstream end of the plate is clamped into a vertical streamlined mast while the three other edges are free. For low velocities  $U$ , the plate is planar and parallel to the air flow. Then, as  $U$  is increased, two-dimensional flutter of the plate spontaneously appears at a critical value  $U_c$  depending on the plate dimensions.

Figures 2 and 3 show superimposed views of the side edge of the plates during one flutter period, captured just at the threshold  $U_c$  for both plates. Such figures allow to visualize the envelope of the flutter motion. Images are captured with a high speed camera parallel to the  $Z$ -axis (see Fig. 1), the air flow is from left to right. These visualizations reveal that different flutter modes can take place at the threshold as the plate dimensions are varied. For the material considered here, the two figures show a change of the mode shape from a single-neck (Fig. 2) to a double-neck (Fig. 3) envelope when the length is increased from 8 to 21 cm. It should be pointed out that these two flutter modes differ not only by the envelope shape but also by the flapping frequency: the measured flutter frequency for the mode shown in Fig. 2 is of 29 Hz, and of 5.6 Hz for the longest plate (Fig. 3).

## Excitation of Shear Layer Instability at Low Reynolds Number via an Unsteady Inflow

Mittal, S.\*

\* Department of Aerospace Engineering, Indian Institute of Technology Kanpur,  
UP 208 016, India. E-mail: smittal@iitk.ac.in

Received 23 March 2006

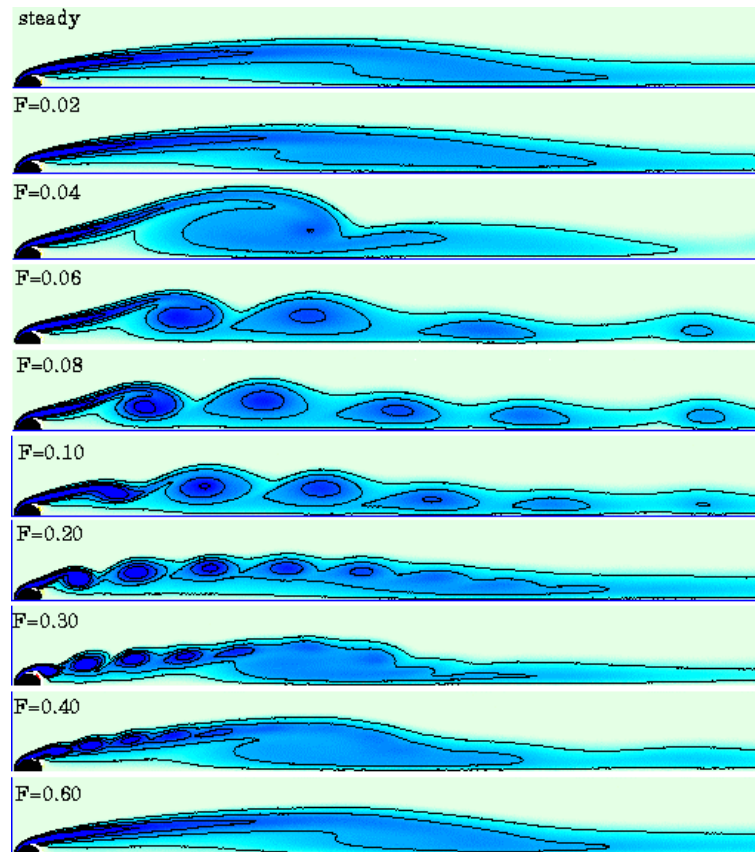


Fig. 1.  $Re = 300$  flow past half a cylinder: vorticity fields for the fully developed flow for the steady inflow (top frame) and unsteady inflow for various  $F$ . The perturbation of the flow speed at the inlet is 1 % of the mean. Red color indicates counter-clockwise while the blue color shows clockwise vorticity.

The Reynolds number for the onset of the shear layer stability in the wake of the cylinder has been a topic of debate in the past. Here, we investigate the instability of the separated shear layer for the  $Re = 300$  flow via an unsteady inflow:  $U_{\text{mean}} [1 + 0.01 \sin(2\pi F t)]$ . To suppress the primary wake instability only one half of the flow past a cylinder is considered with symmetry boundary conditions at the wake center line. The flow with steady inflow is found to be stable (top frame of Fig. 1). The vorticity field for various values of non-dimensional frequency of the perturbation at the inlet,  $F$ , is shown in Fig 1. The shear layer instability is excited for a large range of  $F$ . While the vortices are large for low values of  $F$  they are smaller and spaced closer to each other for higher values of  $F$ . In all cases the dominant frequency of the unsteadiness corresponds to the excitation frequency. All these observations point to the shear layer instability being convective in nature. From the time histories of the oscillations in the flow in the wake it is observed that the instability is strongest for  $F \sim 0.25$ . The computations have been carried out using a stabilized finite element formulation. The mesh consists of 99,014 nodes and 197,164 triangular elements. A stabilized finite element method has been utilized for computing the flow modeled by the incompressible Navier-Stokes equations.

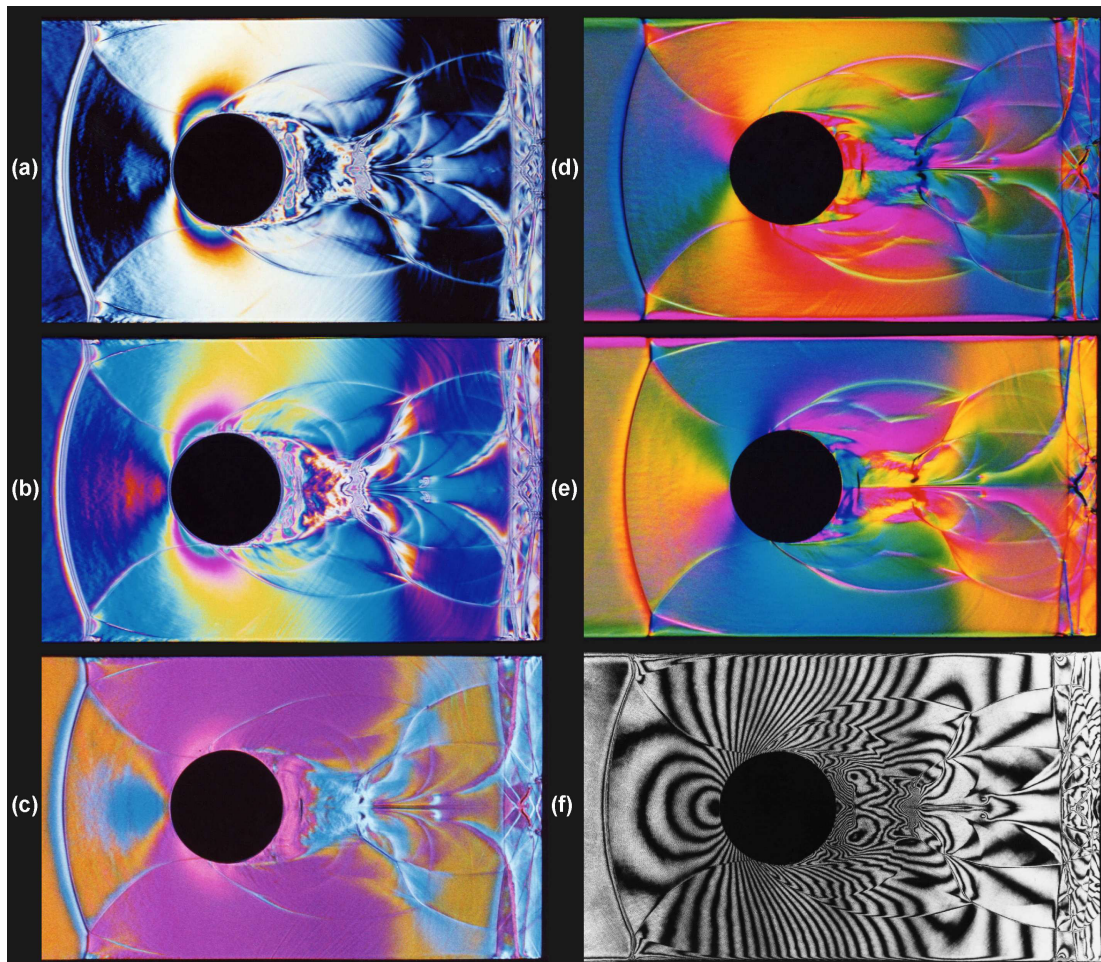
## Shock Wave Diffraction around a Cylinder with Subsequent Reflection from the Shock Tube End Wall

Kleine, H.\*

\* School of Aerospace, Civil and Mechanical Engineering, University of New South Wales, Australian Defence Force Academy, Northcott Drive, Canberra, ACT 2600, Australia.

E-mail: h.kleine@adfa.edu.au

Received 20 May 2006



The images above show a shock wave, initially travelling with a Mach number of 2.25 in  $N_2$ , after it has diffracted around a cylinder (diameter 20 mm) and reflected from the end wall of the shock tube, located 45 mm behind the cylinder. This process has been visualized by four different density-sensitive techniques, each of which depicts the features of the flow differently. Figures (a) and (b) are infinite-fringe shearing interferograms (vertical shear; different fringes were selected for the zero-order background fringe), while Fig. (c) is a color schlieren image, where the colors represent the *magnitude* of the density gradient in flow direction. Figures (d) and (e) are also color schlieren visualizations, but here the colors show the *direction* of the density gradient rather than the magnitude of one of its components. While this introduces a certain degree of asymmetry to the image (the flow is almost perfectly symmetrical with respect to the horizontal centre axis), all the density gradients appearing in this flow become visible. Note that, for example, the boundary layers on the shock tube wall are invisible in Figs. (a)-(c). Figure (f) is a reconstructed holographic interferogram (infinite fringe setting) that shows the density distribution of the flow.